

SLARM: Streaming and Language-Aligned Reconstruction Model for Dynamic Scenes

Zhicheng Qiu^{*†}, Jiarui Meng^{*}, Tong-an Luo^{*}, Yican Huang, Xuan Feng, Xuanfu Li[‡], Zhan Xu
Huawei Technologies Ltd.

{chiu.chih.cheng, mengjiarui, luotongan, huangyican, fengxuan18, lixuanfu, zhan.xu}@huawei.com

^{*} denotes equal contribution, [†] denotes project lead, [‡] denotes corresponding author

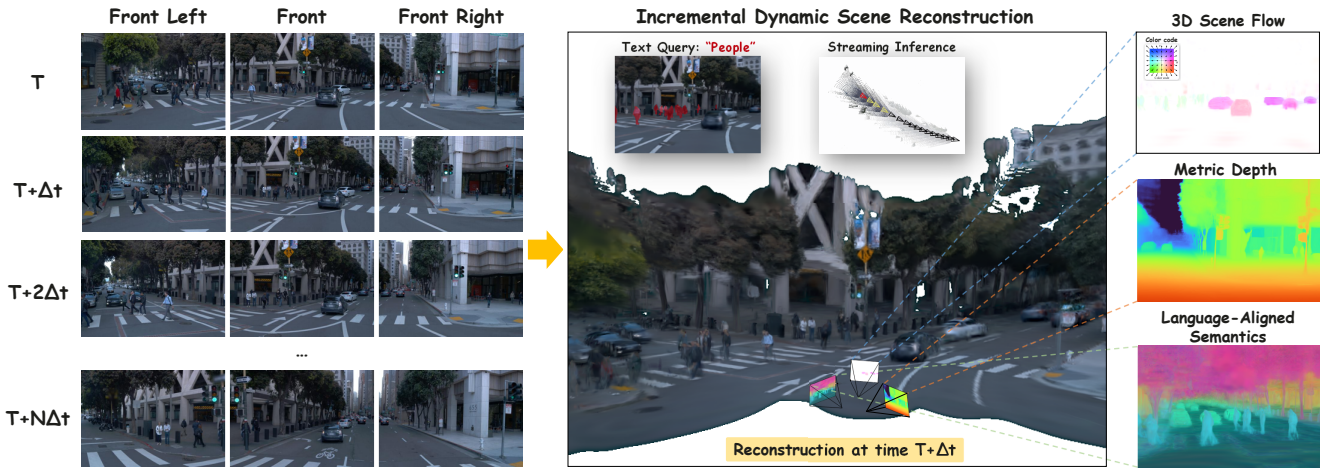


Figure 1. **SLARM** is a large feedforward Transformer using a self-supervised approach for fast and accurate inference of 3D scene flow, metric depth and language-aligned semantics in dynamic scenes. For real-time inference deployment in autonomous driving and embodied AI applications, our model also supports incremental streaming inference.

Abstract

We propose **SLARM**, a feed-forward model that unifies **dynamic scene reconstruction**, **semantic understanding**, and **real-time streaming inference**. **SLARM** captures complex, non-uniform motion through higher-order motion modeling, trained solely on differentiable renderings without any flow supervision. Besides, **SLARM** distills semantic features from LSeg to obtain language-aligned representations. This design enables semantic querying via natural language, and the tight coupling between semantics and geometry further enhances the accuracy and robustness of dynamic reconstruction. Moreover, **SLARM** processes image sequences using window-based causal attention, achieving stable, low-latency streaming inference without accumulating memory cost. Within this unified framework, **SLARM** achieves state-of-the-art results in dynamic estimation, rendering quality, and scene parsing, improving motion accuracy by **21%**, reconstruction PSNR by **1.6 dB**, and segmentation mIoU by **20%** over existing methods.

1. Introduction

The advent of neural radiance fields (NeRF) [38] and 3D Gaussian Splatting (3DGS) [25] has significantly advanced the efficiency and practicality of 3D scene reconstruction. Building on these advances, research has extended to dynamic scene reconstruction [14, 17, 36, 43, 66, 67, 71, 72], enabling new possibilities for immersive interaction and experience. However, existing approaches typically require optimization times ranging from several minutes to several hours and are often limited to per-scene overfitting, with limited ability to generalize across scenes.

Recently, the rise of feed-forward models such as DUST3R [55] and PixelSplat [3] has brought data-driven paradigms into 3D reconstruction. In particular, works like VGGT [53] and MapAnything [24] have challenged the conventional optimization-based reconstruction pipeline, further evolving into general-purpose 3D foundation models. Nevertheless, current approaches remain largely confined to static scenes, and feed-forward reconstruction of dynamic environments remains underexplored.

A recent work STORM [68] enables dynamic 3D scene reconstruction from multi-timestep, posed images. However, it suffers from several key limitations: (1) **oversimplified motion modeling**—it assumes constant-velocity motion, which fails to capture the complex, nonlinear dynamics prevalent in real-world scenes; (2) **limited functionality**—it focuses solely on geometric reconstruction and lacks high-level semantic understanding, hindering its applicability to downstream perception and reasoning tasks; (3) **inefficient inference**—it requires batching multiple input frames and relies on interpolation across timesteps, lacking the capability for incremental, streaming inference.

To address these shortcomings, we propose **SLARM**, a unified 4D Gaussian reasoning framework that simultaneously achieves **dynamic reconstruction**, **semantic understanding**, and **streaming inference**. Our main contributions are summarized as follows.

□ **Accurate and Efficient Motion Modeling**: We propose a motion representation based on a higher-order motion function, enabling effective modeling of non-uniform motion without explicit supervision and significantly improving geometric and dynamic fidelity.

□ **Language-Aligned 4D Semantics**: We distill language-aligned semantic knowledge from 2D foundation model LSeg into the SLARM model, endowing it with text-aligned semantic features that are directly queryable by large language models (LLMs), thereby achieving better dynamic scene understanding and reasoning.

□ **Streaming Inference Architecture**: We process each frame independently and incorporate window-based attention to achieve constant low-latency streaming inference—eliminating the need for batched or sliding-window processing and supporting long-horizon, low-latency deployment in real-world scenarios such as autonomous driving and embodied AI.

□ **Unified Multi-Task Learning**: We jointly optimize geometry, motion, and semantics within a single forward pass, enabling mutual task enhancement and outperforming specialized methods in reconstruction fidelity, motion accuracy, and semantic alignment.

2. Related Work

4D Dynamic Scene Reconstruction. Early dynamic modeling efforts incorporated temporal information into NeRF [11, 40, 43, 63] but suffered from slow training and rendering. Recent works leverage 3D Gaussians for efficiency: 4DGT [65] learns a 4D Gaussian transformer from monocular videos but requires dense 3D supervision; MoVieS [32] achieves fast dynamic view synthesis but depends on precomputed 4D point trajectories or multi-view stereo; STORM [68] models outdoor dynamics via Gaussian motion but assumes linear motion, failing on complex non-rigid motions. Other dynamic ap-

proaches [4, 13, 18, 21, 23, 31, 64, 75] either rely on strong supervision, impose restrictive motion priors, or are constrained by specific inputs. SLARM requires only 2D renderings and camera poses, implicitly learning scene flow through temporal consistency of Gaussian attributes (position, covariance, opacity). It uses learned, non-parametric temporal deformations to capture arbitrary motion patterns without restrictive priors. Pi3 [57] addresses dynamics via permutation-equivariant geometry learning but only produces per-frame reconstructions, lacking inter-frame correspondences for motion reasoning. In contrast, SLARM explicitly models temporal Gaussian motion to yield dense, differentiable flow fields for downstream control. Novel view synthesis methods [20, 22, 35, 58, 77] have focused on photorealism or generation to the exclusion of dynamic 3D modeling.

Semantic 3D Understanding and Language Alignment.

Semantic 3D reconstruction has advanced with vision-language models. LERF [26] pioneered distilling 2D CLIP [45] features into 3D radiance fields. With 3DGS, [29, 44, 48, 60, 70, 73, 74, 80] improved semantic-geometric modeling but relied on per-scene optimization or added computational overhead. Efficient feed-forward methods [10, 19, 56] had limitations in reconstruction quality or robustness. Uni3R [50] unified static 3D reconstruction and language-aligned semantics via 3DGS but lacked temporal modeling. SLARM extends semantic capability to 4D scenes by distilling LSeg features into time-consistent Gaussian descriptors, enabling language-queryable dynamics. Unlike closed-set [47, 79] methods, it enables zero-shot generalization and seamless LLM integration for high-level reasoning in dynamic scenes.

Streaming and Real-Time 3D Perception. Real-time 3D reconstruction is critical for robotics and autonomous systems. SLAM-based methods [8, 33, 37] prioritize accuracy but face latency and speed-precision trade-offs; memory pool-based approaches [12, 52, 61] struggle with temporal fusion or dynamic scene robustness; sequential models [27, 54, 81] suffer from long-range dependency limitations or dynamic adaptability issues. SLARM overcomes these via a pure streaming paradigm: it processes each frame independently while propagating a compact hidden state, ensuring constant latency and memory usage.

3. Method

Task Definition. Given a video sequence $\{\mathbf{I}_t \in \mathbb{R}^{H \times W \times 3}\}_{t=1}^T$ with known camera intrinsics $\mathbf{K}_t \in \mathbb{R}^{3 \times 3}$ and extrinsics $\mathbf{P}_t \in \mathbb{SE}(3)$, our goal is to achieve incremental dynamic scene reconstruction using a feedforward model. To this end, we propose **SLARM**, which maintains an explicit **4D Gaussian Splatting (4DGS)** representation at each time step t that simultaneously: (i) reconstructs current geometry and appearance; (ii) encodes per-Gaussian

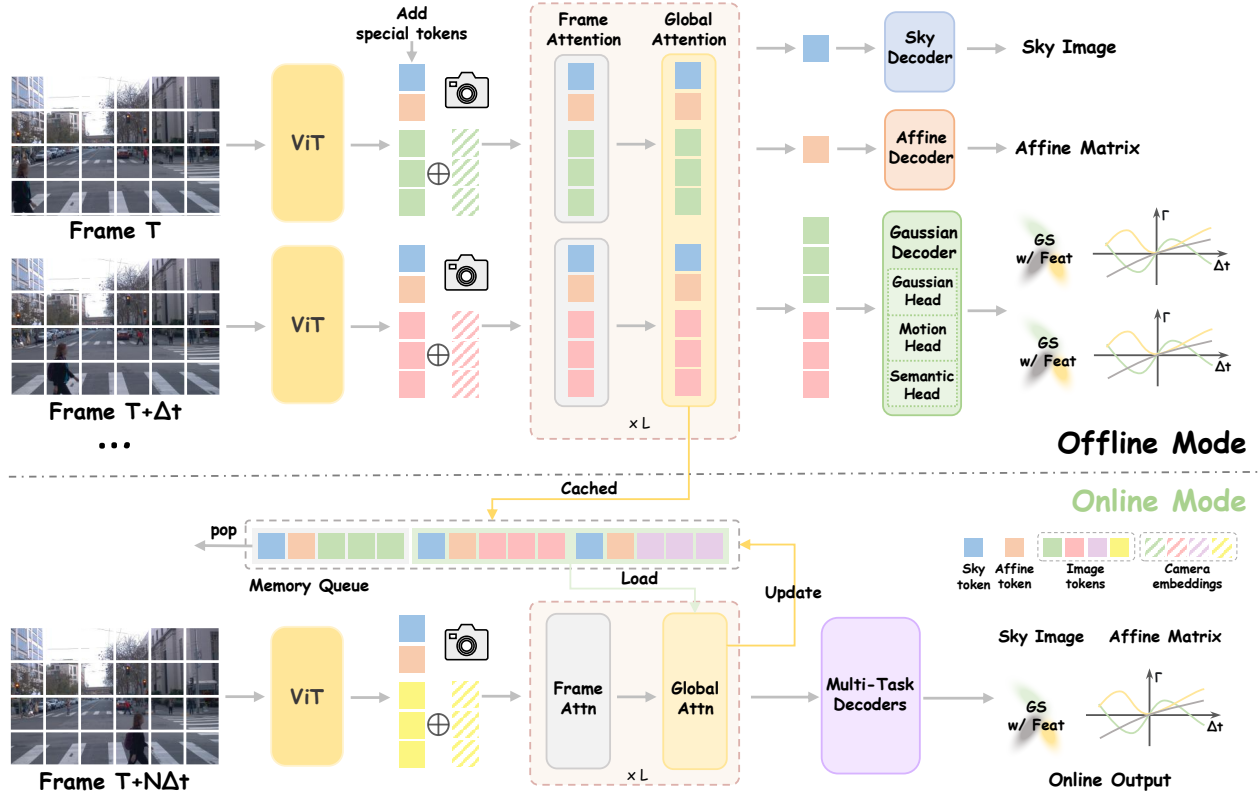


Figure 2. Pipeline of our SLARM model for streaming 4D Gaussian reconstruction. The SLARM model begins by extracting image tokens using a shared-weight Vision Transformer (ViT), and then appending special tokens to these image tokens. These tokens then undergo Frame Attention and Global Attention mechanisms, before being fed into the corresponding decoders to output the parameters.

3D scene flow; and (iii) associates each Gaussian with a language-aligned semantic feature for text-based querying. This formulation addresses three core challenges: unsupervised scene flow learning, vision–language grounding of geometric primitives, and constant-latency, history-aware incremental updates.

3.1. SLARM

Our method, **SLARM**, follows the pipeline illustrated in Figure 2. Given a video sequence $\{\mathbf{I}_t\}_{t=1}^T$, we first extract visual features using a Vision Transformer (ViT), where each frame \mathbf{I}_t is partitioned into non-overlapping patches. To inject geometric priors, we encode each pixel’s viewing ray as a 6D Plücker coordinate [42] derived from known camera intrinsics and extrinsics, linearly project it, and add it to the corresponding visual tokens. Temporal context is incorporated through a learnable embedding of the absolute timestamp t [41]. Following STORM [68], we further concatenate two specialized tokens: a *Sky token* to model the background sky region and an *Affine token* to compensate for exposure and white-balance variations across multi-view cameras. The resulting enriched token sequence is then processed by an *Alternating-Attention Transformer* backbone [53], which alternates between frame-wise and

global self-attention to effectively capture spatio-temporal structure.

Gaussian Decoder regresses a **pixel-aligned 4DGS** representation: for each pixel, it predicts 3D position $\boldsymbol{\mu} \in \mathbb{R}^3$, rotation $\mathbf{q} \in \mathbb{R}^4$, scale $\mathbf{s} \in \mathbb{R}^3$, opacity $\alpha \in [0, 1]$, and color $\mathbf{c} \in \mathbb{R}^3$. The position is computed as $\boldsymbol{\mu} = \mathbf{o} + d \cdot \mathbf{r}$, where $d \in \mathbb{R}$ is predicted depth and $\mathbf{o}, \mathbf{r} \in \mathbb{R}^3$ are the ray origin and direction derived from the camera pose. Two auxiliary heads further predict: (i) a dynamic attribute vector encoding scene flow; and (ii) a semantic feature vector aligned with a vision–language embedding space. All outputs are per-frame and pixel-aligned, enabling direct 2D–3D correspondence and incremental reconstruction. More model architecture details are in the **Supplementary Material**.

We next detail our approach along three aspects: (1) self-supervised dynamic modeling without ground truth scene flows; (2) language-aligned semantics via distillation from 2D foundation models; and (3) streaming inference via incremental state propagation.

3.2. Dynamic Representation and Learning

Previous optimization-based approaches to dynamic scene modeling commonly formulate motion using time-dependent displacement field, which requires precise

estimation of the object’s position at each individual timestamp, resulting in low prediction accuracy in real scene. To alleviate this requirement, STORM [68] adopts a velocity-based formulation by predicting instantaneous object velocities. However, it relies on the assumption of constant velocity over time, which is insufficient to model complex, non-uniform motion patterns such as those observed in human limbs, as shown in Figure 5(a).

High-Order Motion Modeling. To overcome these limitations, we model displacement as a differentiable function of time using a multi-order Taylor expansion. Specifically, for each order $l \in \{0, \dots, L-1\}$, the network predicts a scalar speed $s_l \in \mathbb{R}$ and a 3D directional vector $\mathbf{v}_l \in \mathbb{R}^3$. The directional vector is L2-normalized, and the resulting motion coefficient $\mathbf{m}_l \in \mathbb{R}^3$ is computed as

$$\mathbf{m}_l = s_l \cdot \frac{\mathbf{v}_l}{\|\mathbf{v}_l\|_2}. \quad (1)$$

Given a temporal offset Δt , the total displacement is then obtained by aggregating contributions from all orders in a Taylor-like expansion up to the L -th order:

$$\mathbf{\Gamma}(\Delta t) = \sum_{l=0}^{L-1} \frac{\mathbf{m}_l \cdot (\Delta t)^{l+1}}{(l+1)!}. \quad (2)$$

We adopt $L = 3$ in our experiments, corresponding to a **3rd-order** expansion that explicitly models the first three temporal derivatives of position—velocity, acceleration, and jerk—offering a compact yet expressive representation for complex real-world dynamics.

Rendering-Supervised Motion Learning. Our approach learns scene motion in a fully self-supervised manner without requiring ground-truth scene flow. Specifically, given an input frame at time t and a supervision frame at time $t + \Delta t$, the network predicts the forward scene flow $\mathbf{\Gamma}(\Delta t)$ that maps each 3D Gaussian position from time t to $t + \Delta t$.

Let $\mathcal{G}_t = \{\boldsymbol{\mu}_i, \alpha_i, \mathbf{q}_i, \mathbf{s}_i, \mathbf{c}_i\}_{i=1}^N$ denote the set of 3D Gaussians at time t . We only allow the positions to evolve over time, keeping all other attributes fixed. The transformed Gaussians at time $t + \Delta t$ are thus:

$$\mathcal{G}_{t \rightarrow t+\Delta t} = \{\boldsymbol{\mu}_i + \mathbf{\Gamma}_i(\Delta t), \alpha_i, \mathbf{q}_i, \mathbf{s}_i, \mathbf{c}_i\}_{i=1}^N. \quad (3)$$

We render this warped Gaussian set to obtain a synthesized image $\hat{\mathbf{I}}_{t+\Delta t}$. The motion prediction is supervised by a combination of pixel-wise MSE and perceptual LPIPS loss against the ground-truth supervision frame $\mathbf{I}_{t+\Delta t}$:

$$\mathcal{L}_{\text{rgb}} = \|\hat{\mathbf{I}}_{t+\Delta t} - \mathbf{I}_{t+\Delta t}\|_2^2 + \lambda_{\text{lpiips}} \cdot \text{LPIPS}(\hat{\mathbf{I}}_{t+\Delta t}, \mathbf{I}_{t+\Delta t}), \quad (4)$$

where λ_{lpiips} is set to 0.05.

3.3. Semantic Feature Distillation

Our approach extends the semantic distillation framework to a dynamic setting, where 2D semantic information is distilled into a **4DGS** representation. This extension not only enhances the model’s ability to understand dynamic scenes but also leverages semantic consistency to improve motion estimation accuracy.

Extending 2D semantics to 4D Gaussian primitives. Similar to Uni3R [50], each Gaussian primitive in our model is augmented with a high-dimensional semantic feature vector $\mathbf{f}_j^{\text{sem}} \in \mathbb{R}^d$. However, different from the static 3D representation in Uni3R, our Gaussians evolve over time according to the higher-order motion function $\mathbf{\Gamma}$. During rendering, we synthesize both RGB images and semantic feature maps $\hat{\mathbf{F}}_{t+\Delta t} \in \mathbb{R}^{h \times w \times d}$ at supervision frame at timestamps $t + \Delta t$ by alpha-blending the semantic attributes of time-warped Gaussians.

To supervise this 4D semantic field, we extract per-frame 2D semantic features $\tilde{\mathbf{F}}_{t+\Delta t} \in \mathbb{R}^{h \times w \times c}$ using the frozen 2D foundation model LSeg [28]. The distillation loss is defined as the MSE between rendered and 2D features:

$$\mathcal{L}_{\text{sem}} = \|\tilde{\mathbf{F}}_{t+\Delta t} - \hat{\mathbf{F}}'_{t+\Delta t}\|_2^2, \quad (5)$$

where $\hat{\mathbf{F}}'_{t+\Delta t} \in \mathbb{R}^{h \times w \times c}$ is the decoded semantic map from a lightweight MLP for reducing memory usage.

Enhancing semantic reconstruction with semantically annotated data.

For data with existing semantic annotations, we aim to leverage such data effectively to further enhance semantic reconstruction performance. Since we distill features from LSeg, we opt to utilize semantically annotated data in the same manner as it.

As is illustrated in the right part of Figure 3, reconstructed semantics are decoded into a feature map with width w and height h . We then calculate the similarities between each feature $\mathbf{f}_{ij} \in \mathbb{R}^c$ in this feature map and the text feature $\mathbf{t}_k \in \mathbb{R}^c$ of each category (extracted using the CLIP text encoder) via the inner product, and convert these similarities into category probabilities via softmax. At this point, this reduces to a classification task, for which we employ cross-entropy loss:

$$\mathcal{L}_{\text{cls}} = \frac{1}{hw} \sum_{i,j=1}^{h,w} -\log \left(\frac{\exp(\mathbf{f}_{ij} \cdot \mathbf{t}_{k_{ij}}/\tau)}{\sum_{k=1}^K \exp(\mathbf{f}_{ij} \cdot \mathbf{t}_k/\tau)} \right), \quad (6)$$

where k_{ij} denotes the ground-truth category of the feature at position (i, j) , and τ is a user-defined temperature parameter that we set to 0.07 (the same as that in LSeg).

3.4. Streaming 4D Scene Reconstruction

In contrast to streaming methods like StreamVGGT [81] and Stream3R [27], which reconstruct only per-frame 3D

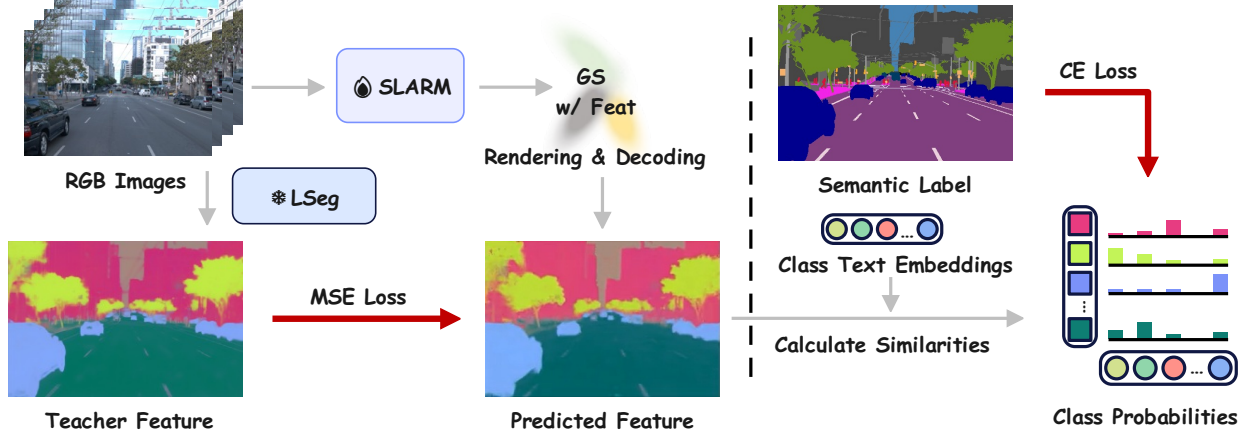


Figure 3. Illustration of semantic supervision in SLARM. Left: Self-supervised feature learning via distillation from LSeg, where rendered semantic Gaussians are decoded. Right: Supervised training on labeled data by aligning predictions with class text embeddings.

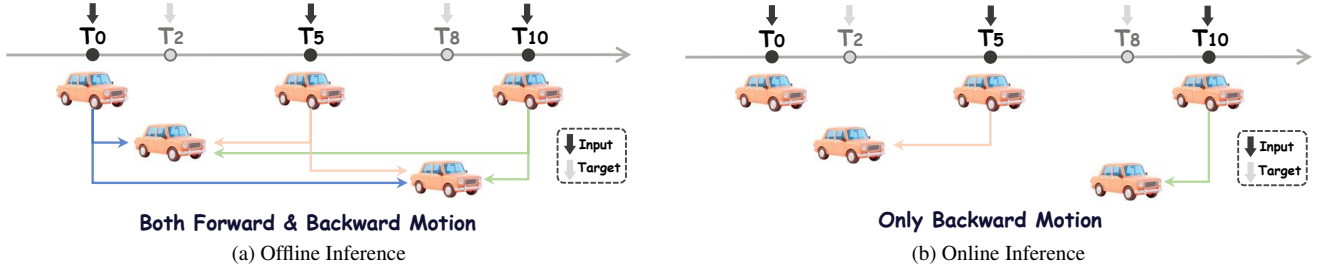


Figure 4. Illustration of motion handling for dynamic Gaussians under two modes. In offline inference, the target frame is synthesized by interpolating all input frames. In online inference, the target frame is reconstructed via backward warping from the subsequent frame.

geometry, we tackle **streaming 4D scene reconstruction**—jointly modeling instantaneous geometry and its continuous temporal deformation under real-time latency and memory constraints. Unlike offline dynamic reconstruction methods that interpolate using both past and future frames, our approach adheres to strict causality: at inference, only current and past observations are available. This requires retroactively refining dynamic content by propagating Gaussian primitives backward in time, while preserving static elements for geometric consistency.

Formally, under the streaming setting, our model outputs both the 3D Gaussian representation \mathcal{G}_t and the associated displacement field $\Delta\mu_t$ at time t , conditioned exclusively on the observed frames up to the current timestamp:

$$(\mathcal{G}_t, \Gamma_t) = \phi(\mathbf{I}_t \mid \mathbf{I}_{t-\Delta t}, \mathbf{I}_{t-2\Delta t}, \dots), \quad (7)$$

where ϕ denotes our causal streaming reconstructor, and Δt is the temporal stride (typically $\Delta t = 5$).

As illustrated in Figure 4(b), the dynamic Gaussians in \mathcal{G}_t are propagated backward only to the most recent historical frame at time $t - \Delta t$. Consequently, the scene representation over the interval $[t - \Delta t, t]$ is composed of two disjoint components:

$$\mathcal{S}_{[t-\Delta t, t]} = \underbrace{\mathcal{G}_{t-\Delta t}^{\text{static}} \cup \mathcal{G}_t^{\text{static}}}_{\text{static geometry}} \cup \underbrace{\mathcal{G}_{t \rightarrow t-\Delta t}^{\text{dynamic}}}_{\text{backward dynamics}}, \quad (8)$$

where $\mathcal{G}_{t-\Delta t}^{\text{static}}$ denotes the static subset of Gaussians from timestamp $t - \Delta t$. Specifically, each Gaussian primitive $g = (\mu, \alpha, \mathbf{q}, \mathbf{s}, \mathbf{c}) \in \mathcal{G}$ is associated with a displacement field Γ_g . We partition \mathcal{G} into static and dynamic subsets based on motion magnitude:

$$\begin{aligned} \mathcal{G}^{\text{static}} &= \{g \in \mathcal{G} \mid \|\Gamma_g(\Delta t)\| \leq \tau_m\}, \\ \mathcal{G}^{\text{dynamic}} &= \{g \in \mathcal{G} \mid \|\Gamma_g(\Delta t)\| > \tau_m\}, \end{aligned} \quad (9)$$

where $\tau_m > 0$ is a motion threshold. The above design enables streaming inference and prevents rendering holes at new timesteps.

3.5. Implementation Details

Training. We train the model for 4 days on 64 Huawei Ascend 910B NPUs with a batch size of 64, using the AdamW [34] optimizer to minimize the training loss over 200k iterations.

Supervision and Loss Functions. After aggregating the input frames (observations) across time into an amodal 4D scene representation, we can render the scene at any target timestamp within the observed temporal window. During training, we randomly sample multiple interpolation timestamps within this window for supervision. For each rendered frame, we optimize the following composite loss:

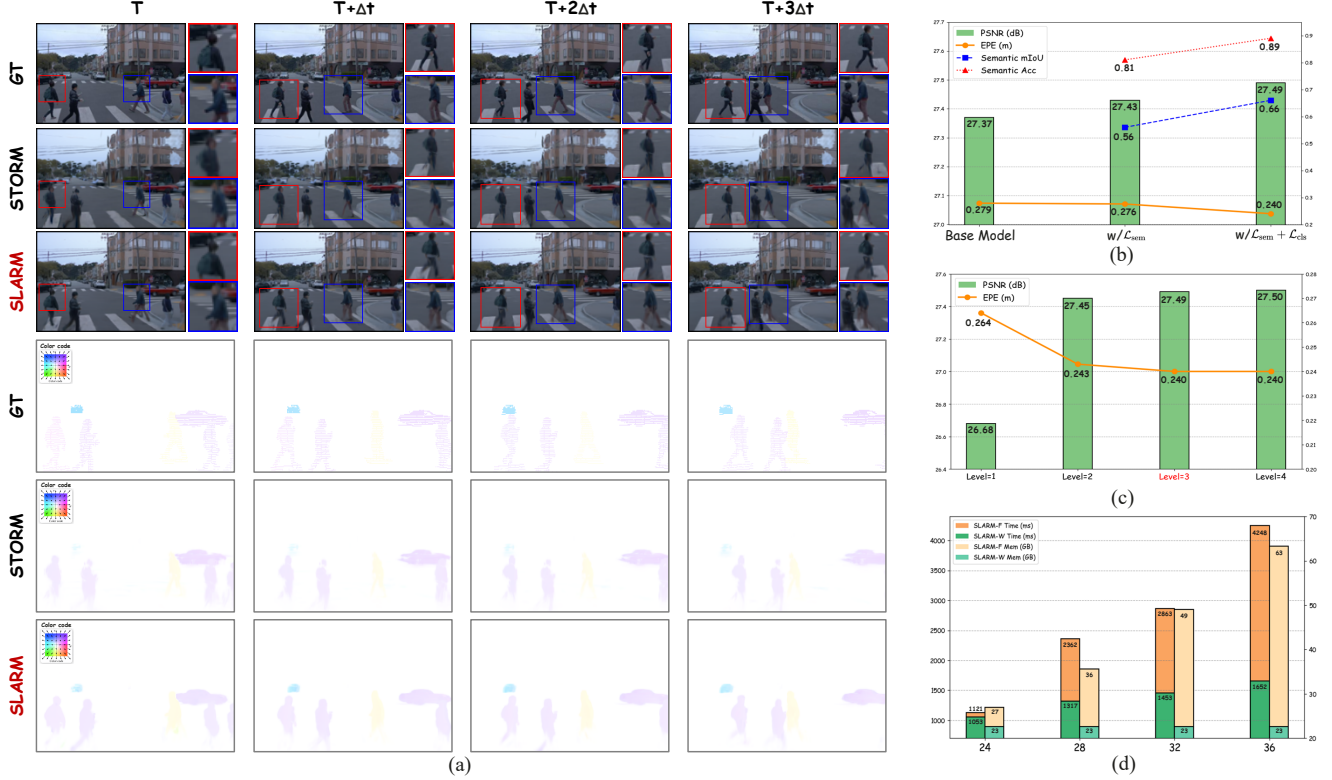


Figure 5. (a) Qualitative comparison of dynamic scenes. (b) Influence of different semantic loss terms on model performance. (c) Impact of varying motion levels on model performance. (d) Comparison of inference speed and memory usage between online and offline modes.

$$\mathcal{L}_{\text{total}} = \mathcal{L}_{\text{rgb}} + \mathcal{L}_{\text{depth}} + \lambda_{\text{sky}} \mathcal{L}_{\text{sky}} + \lambda_{\text{reg}} \mathcal{L}_{\text{reg}} + \lambda_{\text{feat}} \mathcal{L}_{\text{feat}}, \quad (10)$$

where the individual loss terms are defined as follows.

The depth consistency loss enforces geometric alignment with the ground-truth depth map $\mathbf{D}_{\text{gt}} \in \mathbb{R}^{H \times W}$:

$$\mathcal{L}_{\text{depth}} = \frac{1}{|\mathbf{M}_{\text{valid}}|} \sum_{p \in \mathbf{M}_{\text{valid}}} \|\hat{\mathbf{D}}_p - \mathbf{D}_{\text{gt},p}\|_1, \quad (11)$$

where $\mathbf{M}_{\text{valid}}$ is the set of valid pixel indices that have corresponding depth values in \mathbf{D}_{gt} . Specifically, $\mathbf{D}_{\text{gt},p}$ and $\hat{\mathbf{D}}_p$ denote the ground-truth and predicted depth values at pixel p , respectively.

The sky regularization loss encourages transparency in sky regions by penalizing the predicted opacity values in the rendered alpha map $\hat{\mathbf{A}} \in \mathbb{R}^{H \times W}$. The sky mask \mathbf{M}_{sky} is obtained from DepthAnythingV2 [69] by selecting pixels with zero depth. The loss is computed only over these sky pixels:

$$\mathcal{L}_{\text{sky}} = \frac{1}{|\mathbf{M}_{\text{sky}}|} \sum_{p \in \mathbf{M}_{\text{sky}}} \hat{\mathbf{A}}_p, \quad (12)$$

where $\hat{\mathbf{A}}_p$ denotes the predicted alpha (opacity) at pixel p , and $|\mathbf{M}_{\text{sky}}|$ is the number of sky pixels.

A motion regularization term suppresses higher-order coefficients under the prior that most scenes are static:

$$\mathcal{L}_{\text{reg}} = \sum_{l=0}^3 \|\mathbf{m}_l\|_2^2. \quad (13)$$

The feature alignment loss is given by:

$$\mathcal{L}_{\text{feat}} = \mathcal{L}_{\text{sem}} \vee \mathcal{L}_{\text{cls}}, \quad (14)$$

where \vee denotes “or”. In our final training protocol, we first optimize the model using \mathcal{L}_{sem} as $\mathcal{L}_{\text{feat}}$ for 200k iterations, followed by an additional 3k iterations with \mathcal{L}_{cls} substituted for $\mathcal{L}_{\text{feat}}$. Specifically, the loss weights are set to $\lambda_{\text{sky}} = 0.1$, $\lambda_{\text{reg}} = 0.005$, and $\lambda_{\text{feat}} = 1.0$ throughout training.

4. Experiments

Dataset. We conduct our main experiments on the Waymo Open Dataset (WOD) [49], a large-scale autonomous driving benchmark featuring rich dynamics and synchronized multi-camera video sequences. Our experiments use 1,000 driving sequences—798 for training and 202 for validation—each approximately 20 seconds long at 10 fps (yielding ~ 200 frames per sequence). Input images are downsampled by a factor of 8 to 160×240 . To align the resolution of the extracted LSeg [28] features with it, image inputs for feature extraction use 320×480 .

Table 1. **Comparison to state-of-the-art methods on the WOD.** We compare photorealism and geometry metrics against generalizable feed-forward methods. PSNR, SSIM, and Depth RMSE (D-RMSE) are reported. SLARM-F denotes the model using full attention in offline mode, whereas SLARM-W uses window-attention in online mode. *: reproduced by us. †: Non-sky region.

Methods	Dynamic-only			Full image [†]		
	PSNR \uparrow	SSIM \uparrow	D-RMSE \downarrow	PSNR \uparrow	SSIM \uparrow	D-RMSE \downarrow
LGM [51]	17.36	0.216	11.09	18.53	0.447	9.07
LGM* [51]	19.58	0.443	9.43	23.59	0.691	8.02
GS-LRM* [76]	20.02	0.520	9.95	25.18	0.753	7.94
MapAnything [24]	-	-	20.99	-	-	13.53
STORM* [68]	22.03	0.623	7.50	25.86	0.804	5.47
<i>Ours</i>						
SLARM-W	23.20	0.676	6.38	27.30	0.825	4.75
SLARM-F	23.51	0.691	6.16	27.49	0.828	4.57

We present main experimental results and analyses below. More experimental results analyses are provided in the **Supplementary Material**.

4.1. Dynamic Reconstruction

Setup and Baselines. We report standard metrics: PSNR and SSIM for photometric fidelity, and RMSE for depth accuracy. We compare SLARM with existing generalizable feed-forward reconstruction models on the validation split of the WOD [49]. To better understand model behavior in dynamic environments, we further analyze performance separately on the *full image* and on *dynamic regions only* (masked using ground-truth motion annotations).

Results. Quantitative results are summarized in Table 1. SLARM outperforms all generalizable feed-forward methods across all metrics, with consistent gains of 1.6 dB in PSNR on full images and improvements of over 1.5 dB in PSNR and 0.07 in SSIM on dynamic regions—highlighting its superior photorealism and geometric accuracy.

4.2. Flow Estimation

Setup and Baselines. We evaluate flow estimation on the validation split of the WOD [49], which provides ground-truth 3D scene flows. Following the protocol of STORM, we report standard metrics including End-Point Error in 3D (EPE3D), Acc₅, Acc₁₀, and angular error θ_{err} . Notably, while STORM originally evaluates only on input context frames, we adopt a more comprehensive evaluation strategy by considering the entire video sequence—including both input context frames and output interpolated target frames—to enable a fairer and more objective comparison.

Results. As shown in Table 3, SLARM outperforms all competing methods across all metrics, achieving significant improvements particularly in EPE3D and angular error θ_{err} . This demonstrates the importance of higher-order motion modeling for dynamic scene reconstruction. In contrast to STORM, which assumes uniform motion for all scene ob-

Table 2. **Quantitative comparison of semantic segmentation performance.** Our method SLARM achieves the best mIoU and accuracy among all methods.

Method	mIoU \uparrow	Acc \uparrow
EfficientViT-Seg [2]	0.4352	0.7637
Mask2Former-R50 [6]	0.4429	0.7082
SegMAN [16]	0.4567	0.7186
SegFormer [62]	0.4660	0.7572
OffSeg-B [78]	0.4612	0.7417
OffSeg-L [78]	0.4868	0.7635
LSeg [28]	0.4876	0.7976
Mask2Former-Swin [6]	0.5505	0.8192
SLARM	0.6663	0.8923

jects, our method can capture more complex motion patterns, leading to more accurate 3D scene flow predictions.

4.3. Semantic Segmentation in 3D Reconstruction

Setup and Baselines. Following the same protocol as Sec. 4.1, we use semantically annotated validation images from WOD [49] for semantic segmentation evaluation, with standard mIoU and Acc metrics. We compare our method with several SOTA methods, all of which are pre-trained on Cityscapes [7] and spanning diverse cutting-edge paradigms. To ensure a fair comparison, all methods are evaluated at the same image resolution of 160×240 .

Results. Quantitative results are summarized in Table 2. SLARM achieves highly coherent and accurate semantic predictions within the 3D reconstruction pipeline, and outperforms the strong 2D baselines. We attribute this improvement to two key factors: (i) the combination of semantic priors inherited from LSeg and semantic knowledge learned from ground truth, and (ii) the explicit incorporation of 3D geometric priors, which substantially enhance the expressiveness and robustness of learned features.

4.4. Qualitative Results

Dynamic Reconstruction Results. We evaluate on a challenging walking-person scene, as shown in Figure 5(a), where the horizontal axis denotes timesteps. The top three rows show ground-truth RGB, STORM’s reconstruction, and ours. Red/blue boxes highlight two pedestrians, with close-ups for detail. STORM assumes uniform velocity, yielding nearly identical poses across frames and failing to capture natural gait dynamics. In contrast, our higher-order motion modeling accurately reconstructs time-varying pose changes. This is further confirmed by 3D scene flow (bottom three rows): our method captures fine-grained motion variations in speed and direction that STORM misses.

Semantic Segmentation Results. As shown in Table 2 and Figure 6, SLARM achieves state-of-the-art semantic

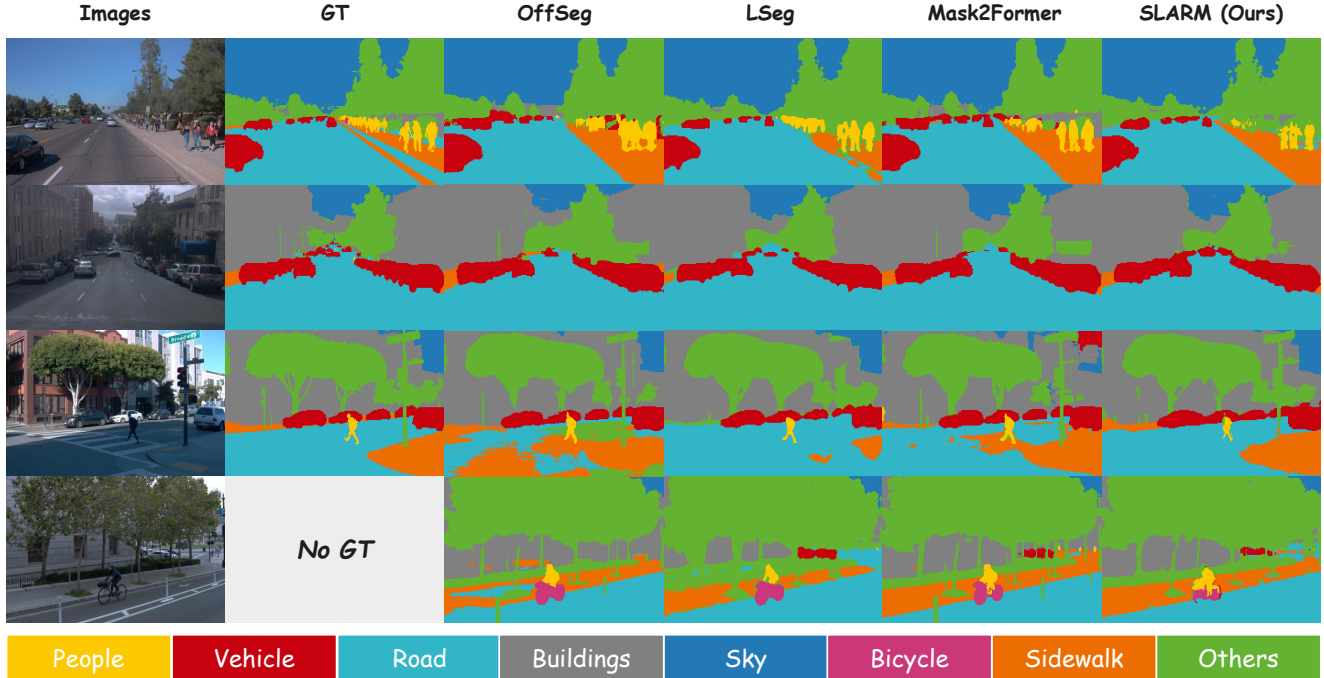


Figure 6. Qualitative comparison of semantic segmentation performance. Our method produces more accurate and coherent segmentations compared to previous 2D segmentation approaches.

segmentation with highly coherent results. We evaluate on common autonomous driving scenarios and key categories, showing strong accuracy on critical classes (e.g., people, vehicle, road, sidewalk) as well as the “others” category—covering safety-relevant objects. All results are obtained by matching language-aligned features with CLIP [45] text embeddings. These semantically rich features can further enhance a large language model’s understanding of dynamic scenes.

Streaming Inference Results. As shown in Figure 5(d), SLARM-W outperforms SLARM-F in inference speed and memory consumption. With window attention, it achieves linear inference time and stable memory usage, making it well-suited for long-sequence streaming inference.

4.5. Ablation Study

High-order motion representation. As introduced in Sec. 3.2, we model dynamics using a high-order motion representation, where increasing orders correspond to higher kinematic derivatives (e.g., velocity, acceleration, jerk). As shown in Figure 5(c), we find that a **3rd-order** model suffices for optimal performance: over short time intervals, real-world motion is well-approximated by jerk-level dynamics, with higher orders yielding diminishing returns.

Enhancing dynamic reconstruction with semantic guidance. We leverage semantic consistency as a temporal regularizer: objects with coherent semantic identity (e.g., cars, pedestrians) should follow smooth, physically plausible trajectories. As shown in Figure 5(b) experiments confirm its

Table 3. Comparison of scene flow estimation on the WOD.

Methods	EPE (m) ↓	Acc ₅ (%) ↑	Acc ₁₀ (%) ↑	θ (rad) ↓
NSFP [30]	0.703	41.03	52.16	0.934
NSFP++ [39]	0.724	51.56	60.04	1.103
STORM [68]	0.304	79.01	83.74	0.667
<i>Ours</i>				
SLARM-F	0.240	78.15	83.08	0.540
SLARM-W	0.337	81.07	84.26	0.725

benefit: \mathcal{L}_{sem} yields a lower Flow EPE metric, and the subsequent adoption of \mathcal{L}_{cls} further reduces it. Furthermore, with improved dynamic performance, PSNR and semantic metrics are correspondingly improved.

5. Conclusion

In this work, we present Streaming and Language-Aligned Reconstruction Model (SLARM), a scalable feed-forward 4D Gaussian Splatting framework that jointly recovers 3D scene flow, metric depth, and language-aligned semantics from posed video. Trained purely via rendering-based self-supervision, SLARM captures complex motion without ground-truth flow and supports real-time incremental inference. The model supports language-aligned semantics, enabling integration with Vision-Language Models (VLMs) for Vision-Language-Action (VLA) systems. However, SLARM currently requires accurate camera poses and struggles with complex materials like glass or mirrors due to its reliance on photometric consistency. Future work will explore self-calibration and more realistic scene representations to address these limitations.

References

- [1] Holger Caesar, Varun Bankiti, Alex H Lang, Sourabh Vora, Venice Erin Liong, Qiang Xu, Anush Krishnan, Yu Pan, Giancarlo Baldan, and Oscar Beijbom. nuscenes: A multi-modal dataset for autonomous driving. In *Proceedings of the IEEE/CVF conference on computer vision and pattern recognition*, pages 11621–11631, 2020. 2
- [2] Han Cai, Junyan Li, Muyan Hu, Chuang Gan, and Song Han. Efficientvit: Lightweight multi-scale attention for high-resolution dense prediction. In *Proceedings of the IEEE/CVF international conference on computer vision*, pages 17302–17313, 2023. 7
- [3] David Charatan, Sizhe Lester Li, Andrea Tagliasacchi, and Vincent Sitzmann. pixelsplat: 3d gaussian splats from image pairs for scalable generalizable 3d reconstruction. In *Proceedings of the IEEE/CVF conference on computer vision and pattern recognition*, pages 19457–19467, 2024. 1
- [4] Xingyu Chen, Yue Chen, Yuliang Xiu, Andreas Geiger, and Anpei Chen. Easi3r: Estimating disentangled motion from dust3r without training. *arXiv preprint arXiv:2503.24391*, 2025. 2
- [5] Xuweiyi Chen, Tian Xia, Sihan Xu, Jianing Yang, Joyce Chai, and Zezhou Cheng. Sab3r: Semantic-augmented backbone in 3d reconstruction. *arXiv preprint arXiv:2506.02112*, 2025. 1
- [6] Bowen Cheng, Ishan Misra, Alexander G Schwing, Alexander Kirillov, and Rohit Girdhar. Masked-attention mask transformer for universal image segmentation. In *Proceedings of the IEEE/CVF conference on computer vision and pattern recognition*, pages 1290–1299, 2022. 7
- [7] Marius Cordts, Mohamed Omran, Sebastian Ramos, Timo Rehfeld, Markus Enzweiler, Rodrigo Benenson, Uwe Franke, Stefan Roth, and Bernt Schiele. The cityscapes dataset for semantic urban scene understanding. In *Proceedings of the IEEE conference on computer vision and pattern recognition*, pages 3213–3223, 2016. 7
- [8] Andrew J Davison, Ian D Reid, Nicholas D Molton, and Olivier Stasse. Monoslam: Real-time single camera slam. *IEEE transactions on pattern analysis and machine intelligence*, 29(6):1052–1067, 2007. 2
- [9] Xiaoyi Dong, Jianmin Bao, Yinglin Zheng, Ting Zhang, Dongdong Chen, Hao Yang, Ming Zeng, Weiming Zhang, Lu Yuan, Dong Chen, et al. Maskclip: Masked self-distillation advances contrastive language-image pretraining. In *Proceedings of the IEEE/CVF conference on computer vision and pattern recognition*, pages 10995–11005, 2023. 1
- [10] Zhiwen Fan, Jian Zhang, Wenyan Cong, Peihao Wang, Renjie Li, Kairun Wen, Shijie Zhou, Achuta Kadambi, Zhangyang Wang, Danfei Xu, et al. Large spatial model: End-to-end unposed images to semantic 3d. *Advances in neural information processing systems*, 37:40212–40229, 2024. 2
- [11] Jiemin Fang, Taoran Yi, Xinggang Wang, Lingxi Xie, XiaoPeng Zhang, Wenyu Liu, Matthias Nießner, and Qi Tian. Fast dynamic radiance fields with time-aware neural voxels. In *SIGGRAPH Asia 2022 Conference Papers*, pages 1–9, 2022. 2
- [12] Xin Fei, Wenzhao Zheng, Yueqi Duan, Wei Zhan, Masayoshi Tomizuka, Kurt Keutzer, and Jiwen Lu. Driv3r: Learning dense 4d reconstruction for autonomous driving. *arXiv preprint arXiv:2412.06777*, 2024. 2
- [13] Haiwen Feng, Junyi Zhang, Qianqian Wang, Yufei Ye, Pengcheng Yu, Michael J Black, Trevor Darrell, and Angjoo Kanazawa. St4rtrack: Simultaneous 4d reconstruction and tracking in the world. *arXiv preprint arXiv:2504.13152*, 2025. 2
- [14] Jiaye Fu, Qiankun Gao, Chengxiang Wen, Yanmin Wu, Siwei Ma, Jiaqi Zhang, and Jian Zhang. Recon-gs: Continuum-preserved gaussian streaming for fast and compact reconstruction of dynamic scenes. *Advances in Neural Information Processing Systems*, 2025. 1
- [15] Stephanie Fu, Mark Hamilton, Laura Brandt, Axel Feldman, Zhoutong Zhang, and William T Freeman. Featup: A model-agnostic framework for features at any resolution. *arXiv preprint arXiv:2403.10516*, 2024. 1
- [16] Yunxiang Fu, Meng Lou, and Yizhou Yu. Segman: Omni-scale context modeling with state space models and local attention for semantic segmentation. In *Proceedings of the Computer Vision and Pattern Recognition Conference*, pages 19077–19087, 2025. 7
- [17] Qiankun Gao, Jiarui Meng, Chengxiang Wen, Jie Chen, and Jian Zhang. Hicom: Hierarchical coherent motion for dynamic streamable scenes with 3d gaussian splatting. *Advances in Neural Information Processing Systems*, 37:80609–80633, 2024. 1
- [18] Jisang Han, Honggyu An, Jaewoo Jung, Takuya Narihira, Junyoung Seo, Kazumi Fukuda, Chaehyun Kim, Sunghwan Hong, Yuki Mitsufuji, and Seungryong Kim. D²ust3r: Enhancing 3d reconstruction with 4d pointmaps for dynamic scenes. *arXiv preprint arXiv:2504.06264*, 2025. 2
- [19] Jie Hu, Shizun Wang, and Xinchao Wang. Pe3r: Perception-efficient 3d reconstruction. *arXiv preprint arXiv:2503.07507*, 2025. 2, 1
- [20] Lihan Jiang, Yucheng Mao, Linning Xu, Tao Lu, Kerui Ren, Yichen Jin, Xudong Xu, Mulin Yu, Jiangmiao Pang, Feng Zhao, et al. Anysplat: Feed-forward 3d gaussian splatting from unconstrained views. *arXiv preprint arXiv:2505.23716*, 2025. 2
- [21] Zeren Jiang, Chuanxia Zheng, Iro Laina, Diane Larlus, and Andrea Vedaldi. Geo4d: Leveraging video generators for geometric 4d scene reconstruction. *arXiv preprint arXiv:2504.07961*, 2025. 2
- [22] Haian Jin, Hanwen Jiang, Hao Tan, Kai Zhang, Sai Bi, Tianyuan Zhang, Fujun Luan, Noah Snavely, and Zexiang Xu. Lvsm: A large view synthesis model with minimal 3d inductive bias. *arXiv preprint arXiv:2410.17242*, 2024. 2
- [23] Linyi Jin, Richard Tucker, Zhengqi Li, David Fouhey, Noah Snavely, and Aleksander Holynski. Stereo4d: Learning how things move in 3d from internet stereo videos. *arXiv preprint arXiv:2412.09621*, 2024. 2
- [24] Nikhil Keetha, Norman Müller, Johannes Schönberger, Lorenzo Porzi, Yuchen Zhang, Tobias Fischer, Arno Knapitsch, Duncan Zauss, Ethan Weber, Nelson Antunes, et al. Mapanything: Universal feed-forward metric 3d reconstruction. *arXiv preprint arXiv:2509.13414*, 2025. 1, 7

- [25] Bernhard Kerbl, Georgios Kopanas, Thomas Leimkühler, and George Drettakis. 3d gaussian splatting for real-time radiance field rendering. *ACM Trans. Graph.*, 42(4):139–1, 2023. 1
- [26] Justin Kerr, Chung Min Kim, Ken Goldberg, Angjoo Kanazawa, and Matthew Tancik. Lrf: Language embedded radiance fields. In *Proceedings of the IEEE/CVF international conference on computer vision*, pages 19729–19739, 2023. 2
- [27] Yushi Lan, Yihang Luo, Fangzhou Hong, Shangchen Zhou, Honghua Chen, Zhaoyang Lyu, Shuai Yang, Bo Dai, Chen Change Loy, and Xingang Pan. Stream3r: Scalable sequential 3d reconstruction with causal transformer. *arXiv preprint arXiv:2508.10893*, 2025. 2, 4
- [28] Boyi Li, Kilian Q Weinberger, Serge Belongie, Vladlen Koltun, and René Ranftl. Language-driven semantic segmentation. *arXiv preprint arXiv:2201.03546*, 2022. 4, 6, 7, 1
- [29] Qijing Li, Jingxiang Sun, Liang An, Zhaoqi Su, Hongwen Zhang, and Yebin Liu. Semanticsplat: Feed-forward 3d scene understanding with language-aware gaussian fields. *arXiv preprint arXiv:2506.09565*, 2025. 2
- [30] Xueqian Li, Jhony Kaesemodel Pontes, and Simon Lucey. Neural scene flow prior. *Advances in Neural Information Processing Systems*, 34:7838–7851, 2021. 8
- [31] Zhengqi Li, Richard Tucker, Forrester Cole, Qianqian Wang, Linyi Jin, Vickie Ye, Angjoo Kanazawa, Aleksander Holynski, and Noah Snavely. Megasam: Accurate, fast and robust structure and motion from casual dynamic videos. In *Proceedings of the Computer Vision and Pattern Recognition Conference*, pages 10486–10496, 2025. 2
- [32] Chenguo Lin, Yuchen Lin, Panwang Pan, Yifan Yu, Honglei Yan, Katerina Fragkiadaki, and Yadong Mu. Movies: Motion-aware 4d dynamic view synthesis in one second. *arXiv preprint arXiv:2507.10065*, 2025. 2
- [33] Yuzheng Liu, Siyan Dong, Shuzhe Wang, Yingda Yin, Yanchao Yang, Qingnan Fan, and Baoquan Chen. Slam3r: Real-time dense scene reconstruction from monocular rgb videos. In *Proceedings of the Computer Vision and Pattern Recognition Conference*, pages 16651–16662, 2025. 2
- [34] Ilya Loshchilov and Frank Hutter. Decoupled weight decay regularization. *arXiv preprint arXiv:1711.05101*, 2017. 5
- [35] Yuanxun Lu, Jingyang Zhang, Tian Fang, Jean-Daniel Nahmias, Yanghai Tsin, Long Quan, Xun Cao, Yao Yao, and Shiwei Li. Matrix3d: Large photogrammetry model all-in-one. In *Proceedings of the Computer Vision and Pattern Recognition Conference*, pages 11250–11263, 2025. 2
- [36] Jonathon Luiten, Georgios Kopanas, Bastian Leibe, and Deva Ramanan. Dynamic 3d gaussians: Tracking by persistent dynamic view synthesis. In *2024 International Conference on 3D Vision (3DV)*, pages 800–809. IEEE, 2024. 1
- [37] Dominic Maggio, Hyungtae Lim, and Luca Carlone. Vggt-slam: Dense rgb slam optimized on the sl(4) manifold. *arXiv preprint arXiv:2505.12549*, 2025. 2
- [38] Ben Mildenhall, Pratul P Srinivasan, Matthew Tancik, Jonathan T Barron, Ravi Ramamoorthi, and Ren Ng. Nerf: Representing scenes as neural radiance fields for view synthesis. *Communications of the ACM*, 65(1):99–106, 2021. 1
- [39] Mahyar Najibi, Jingwei Ji, Yin Zhou, Charles R Qi, Xinchun Yan, Scott Ettinger, and Dragomir Anguelov. Motion inspired unsupervised perception and prediction in autonomous driving. In *European Conference on Computer Vision*, pages 424–443. Springer, 2022. 8
- [40] Keunhong Park, Utkarsh Sinha, Jonathan T Barron, Sofien Bouaziz, Dan B Goldman, Steven M Seitz, and Ricardo Martin-Brualla. Nerfies: Deformable neural radiance fields. In *Proceedings of the IEEE/CVF international conference on computer vision*, pages 5865–5874, 2021. 2
- [41] William Peebles and Saining Xie. Scalable diffusion models with transformers. In *Proceedings of the IEEE/CVF international conference on computer vision*, pages 4195–4205, 2023. 3
- [42] Julius Plucker. Xvii. on a new geometry of space. *Philosophical Transactions of the Royal Society of London*, (155): 725–791, 1865. 3
- [43] Albert Pumarola, Enric Corona, Gerard Pons-Moll, and Francesc Moreno-Noguer. D-nerf: Neural radiance fields for dynamic scenes. In *Proceedings of the IEEE/CVF conference on computer vision and pattern recognition*, pages 10318–10327, 2021. 1, 2
- [44] Minghan Qin, Wanhua Li, Jiawei Zhou, Haoqian Wang, and Hanspeter Pfister. Langsplat: 3d language gaussian splatting. In *Proceedings of the IEEE/CVF Conference on Computer Vision and Pattern Recognition*, pages 20051–20060, 2024. 2
- [45] Alec Radford, Jong Wook Kim, Chris Hallacy, Aditya Ramesh, Gabriel Goh, Sandhini Agarwal, Girish Sastry, Amanda Askell, Pamela Mishkin, Jack Clark, et al. Learning transferable visual models from natural language supervision. In *International conference on machine learning*, pages 8748–8763. PmLR, 2021. 2, 8, 1
- [46] Nikhila Ravi, Valentin Gabeur, Yuan-Ting Hu, Ronghang Hu, Chaitanya Ryali, Tengyu Ma, Haitham Khedr, Roman Rädle, Chloe Rolland, Laura Gustafson, et al. Sam 2: Segment anything in images and videos. *arXiv preprint arXiv:2408.00714*, 2024. 1
- [47] Jonas Schult, Francis Engelmann, Alexander Hermans, Or Litany, Siyu Tang, and Bastian Leibe. Mask3d: Mask transformer for 3d semantic instance segmentation. *arXiv preprint arXiv:2210.03105*, 2022. 2
- [48] Jin-Chuan Shi, Miao Wang, Hao-Bin Duan, and Shao-Hua Guan. Language embedded 3d gaussians for open-vocabulary scene understanding. In *Proceedings of the IEEE/CVF Conference on Computer Vision and Pattern Recognition*, pages 5333–5343, 2024. 2
- [49] Pei Sun, Henrik Kretschmar, Xerxes Dotiwalla, Aurelien Chouard, Vijaysai Patnaik, Paul Tsui, James Guo, Yin Zhou, Yuning Chai, Benjamin Caine, et al. Scalability in perception for autonomous driving: Waymo open dataset. In *Proceedings of the IEEE/CVF conference on computer vision and pattern recognition*, pages 2446–2454, 2020. 6, 7
- [50] Xiangyu Sun, Haoyi Jiang, Liu Liu, Seungtae Nam, Gyeongjin Kang, Xinjie Wang, Wei Sui, Zhizhong Su,

- Wenyu Liu, Xinggang Wang, et al. Uni3r: Unified 3d reconstruction and semantic understanding via generalizable gaussian splatting from unposed multi-view images. *arXiv preprint arXiv:2508.03643*, 2025. 2, 4
- [51] Jiaxiang Tang, Zhaoxi Chen, Xiaokang Chen, Tengfei Wang, Gang Zeng, and Ziwei Liu. Lgm: Large multi-view gaussian model for high-resolution 3d content creation. In *European Conference on Computer Vision*, pages 1–18. Springer, 2024. 7
- [52] Hengyi Wang and Lourdes Agapito. 3d reconstruction with spatial memory. *arXiv preprint arXiv:2408.16061*, 2024. 2
- [53] Jianyuan Wang, Minghao Chen, Nikita Karaev, Andrea Vedaldi, Christian Rupprecht, and David Novotny. Vggt: Visual geometry grounded transformer. In *Proceedings of the Computer Vision and Pattern Recognition Conference*, pages 5294–5306, 2025. 1, 3
- [54] Qianqian Wang, Yifei Zhang, Aleksander Holynski, Alexei A Efros, and Angjoo Kanazawa. Continuous 3d perception model with persistent state. In *Proceedings of the Computer Vision and Pattern Recognition Conference*, pages 10510–10522, 2025. 2
- [55] Shuzhe Wang, Vincent Leroy, Yohann Cabon, Boris Chidlovskii, and Jerome Revaud. Dust3r: Geometric 3d vision made easy. In *Proceedings of the IEEE/CVF Conference on Computer Vision and Pattern Recognition*, pages 20697–20709, 2024. 1
- [56] Xingrui Wang, Cuiling Lan, Hanxin Zhu, Zhibo Chen, and Yan Lu. Gsemplat: Generalizable semantic 3d gaussian splatting from uncalibrated image pairs. *arXiv preprint arXiv:2412.16932*, 2024. 2
- [57] Yifan Wang, Jianjun Zhou, Haoyi Zhu, Wenzheng Chang, Yang Zhou, Zizun Li, Junyi Chen, Jiangmiao Pang, Chunhua Shen, and Tong He. π^3 : Permutation-equivariant visual geometry learning. *arXiv preprint arXiv:2507.13347*, 2025. 2
- [58] Ethan Weber, Norman Müller, Yash Kant, Vasu Agrawal, Michael Zollhöfer, Angjoo Kanazawa, and Christian Richardt. Fillerbuster: Multi-view scene completion for casual captures. *arXiv preprint arXiv:2502.05175*, 2025. 2
- [59] Benjamin Wilson, William Qi, Tanmay Agarwal, John Lambert, Jagjeet Singh, Siddhesh Khandelwal, Bowen Pan, Ratnesh Kumar, Andrew Hartnett, Jhony Kaesemodel Pontes, et al. Argoverse 2: Next generation datasets for self-driving perception and forecasting. In *Thirty-fifth Conference on Neural Information Processing Systems Datasets and Benchmarks Track (Round 2)*. 2
- [60] Yanmin Wu, Jiarui Meng, Haijie Li, Chenming Wu, Yahao Shi, Xinhua Cheng, Chen Zhao, Haocheng Feng, Errui Ding, Jingdong Wang, et al. Opengaussian: Towards point-level 3d gaussian-based open vocabulary understanding. *Advances in Neural Information Processing Systems*, 37:19114–19138, 2024. 2
- [61] Yuqi Wu, Wenzhao Zheng, Jie Zhou, and Jiwen Lu. Point3r: Streaming 3d reconstruction with explicit spatial pointer memory. *arXiv preprint arXiv:2507.02863*, 2025. 2
- [62] Enze Xie, Wenhai Wang, Zhiding Yu, Anima Anandkumar, Jose M Alvarez, and Ping Luo. Segformer: Simple and efficient design for semantic segmentation with transformers. *Advances in neural information processing systems*, 34:12077–12090, 2021. 7
- [63] Hongyi Xu, Thiemo Alldieck, and Cristian Sminchisescu. H-nerf: Neural radiance fields for rendering and temporal reconstruction of humans in motion. *Advances in Neural Information Processing Systems*, 34:14955–14966, 2021. 2
- [64] Tian-Xing Xu, Xiangjun Gao, Wenbo Hu, Xiaoyu Li, Song-Hai Zhang, and Ying Shan. Geometrycrafter: Consistent geometry estimation for open-world videos with diffusion priors. *arXiv preprint arXiv:2504.01016*, 2025. 2
- [65] Zhen Xu, Zhengqin Li, Zhao Dong, Xiaowei Zhou, Richard Newcombe, and Zhaoyang Lv. 4dgt: Learning a 4d gaussian transformer using real-world monocular videos. *arXiv preprint arXiv:2506.08015*, 2025. 2
- [66] Jinbo Yan, Rui Peng, Zhiyan Wang, Luyang Tang, Jiayu Yang, Jie Liang, Jiahao Wu, and Ronggang Wang. Instant gaussian stream: Fast and generalizable streaming of dynamic scene reconstruction via gaussian splatting. In *Proceedings of the Computer Vision and Pattern Recognition Conference*, pages 16520–16531, 2025. 1
- [67] Zhiwen Yan, Chen Li, and Gim Hee Lee. Nerf-ds: Neural radiance fields for dynamic specular objects. In *Proceedings of the IEEE/CVF Conference on Computer Vision and Pattern Recognition*, pages 8285–8295, 2023. 1
- [68] Jiawei Yang, Jiahui Huang, Yuxiao Chen, Yan Wang, Boyi Li, Yurong You, Apoorva Sharma, Maximilian Igl, Peter Karkus, Danfei Xu, et al. Storm: Spatio-temporal reconstruction model for large-scale outdoor scenes. *arXiv preprint arXiv:2501.00602*, 2024. 2, 3, 4, 7, 8
- [69] Lihe Yang, Bingyi Kang, Zilong Huang, Zhen Zhao, Xiaogang Xu, Jiashi Feng, and Hengshuang Zhao. Depth anything v2. *Advances in Neural Information Processing Systems*, 37:21875–21911, 2024. 6
- [70] Shuzhou Yang, Yu Wang, Haijie Li, Jiarui Meng, Yanmin Wu, Xiandong Meng, and Jian Zhang. Hybrid fourier score distillation for efficient one image to 3d object generation. *Visual Intelligence*, 3(1):17, 2025. 2
- [71] Zeyu Yang, Hongye Yang, Zijie Pan, and Li Zhang. Real-time photorealistic dynamic scene representation and rendering with 4d gaussian splatting. *arXiv preprint arXiv:2310.10642*, 2023. 1
- [72] Ziyi Yang, Xinyu Gao, Wen Zhou, Shaohui Jiao, Yuqing Zhang, and Xiaogang Jin. Deformable 3d gaussians for high-fidelity monocular dynamic scene reconstruction. In *Proceedings of the IEEE/CVF conference on computer vision and pattern recognition*, pages 20331–20341, 2024. 1
- [73] Mingqiao Ye, Martin Danelljan, Fisher Yu, and Lei Ke. Gaussian grouping: Segment and edit anything in 3d scenes. In *European conference on computer vision*, pages 162–179. Springer, 2024. 2
- [74] Justin Yu, Kush Hari, Kishore Srinivas, Karim El-Refai, Adam Rashid, Chung Min Kim, Justin Kerr, Richard Cheng, Muhammad Zubair Irshad, Ashwin Balakrishna, et al. Language-embedded gaussian splats (legs): Incrementally building room-scale representations with a mobile robot. In *2024 IEEE/RSJ International Conference on In-*

- telligent Robots and Systems (IROS)*, pages 13326–13332. IEEE, 2024. [2](#)
- [75] Junyi Zhang, Charles Herrmann, Junhwa Hur, Varun Jampani, Trevor Darrell, Forrester Cole, Deqing Sun, and Ming-Hsuan Yang. Monst3r: A simple approach for estimating geometry in the presence of motion. *arXiv preprint arXiv:2410.03825*, 2024. [2](#)
- [76] Kai Zhang, Sai Bi, Hao Tan, Yuanbo Xiangli, Nanxuan Zhao, Kalyan Sunkavalli, and Zexiang Xu. Gs-irm: Large reconstruction model for 3d gaussian splatting. In *European Conference on Computer Vision*, pages 1–19. Springer, 2024. [7](#), [1](#)
- [77] Shangzhan Zhang, Jianyuan Wang, Yinghao Xu, Nan Xue, Christian Rupprecht, Xiaowei Zhou, Yujun Shen, and Gordon Wetzstein. Flare: Feed-forward geometry, appearance and camera estimation from uncalibrated sparse views. In *Proceedings of the Computer Vision and Pattern Recognition Conference*, pages 21936–21947, 2025. [2](#)
- [78] Shi-Chen Zhang, Yunheng Li, Yu-Huan Wu, Qibin Hou, and Ming-Ming Cheng. Revisiting efficient semantic segmentation: Learning offsets for better spatial and class feature alignment. In *Proceedings of the IEEE/CVF International Conference on Computer Vision*, pages 22361–22371, 2025. [7](#)
- [79] Shuaifeng Zhi, Tristan Laidlow, Stefan Leutenegger, and Andrew J Davison. In-place scene labelling and understanding with implicit scene representation. In *Proceedings of the IEEE/CVF International Conference on Computer Vision*, pages 15838–15847, 2021. [2](#)
- [80] Shijie Zhou, Haoran Chang, Sicheng Jiang, Zhiwen Fan, Zehao Zhu, Dejie Xu, Pradyumna Chari, Suyu You, Zhangyang Wang, and Achuta Kadambi. Feature 3dgs: Supercharging 3d gaussian splatting to enable distilled feature fields. In *Proceedings of the IEEE/CVF Conference on Computer Vision and Pattern Recognition*, pages 21676–21685, 2024. [2](#)
- [81] Dong Zhuo, Wenzhao Zheng, Jiahe Guo, Yuqi Wu, Jie Zhou, and Jiwen Lu. Streaming 4d visual geometry transformer. *arXiv preprint arXiv:2507.11539*, 2025. [2](#), [4](#)

SLARM: Streaming and Language-Aligned Reconstruction Model for Dynamic Scenes

Supplementary Material

6. More Implementation Details

Model architecture. As the standard configuration, our model employs a 12-layer Alternating-Attention Transformer [53], which interleaves frame-wise and global self-attention mechanisms. Each attention layer operates with a feature dimensionality of 768. The input image is processed using a Vision Transformer (ViT) with a patch size of 8×8 , yielding a sequence of image tokens that serve as input to a Gaussian Decoder. This decoder comprises three lightweight MLP-based task-specific heads: a *Gaussian head*, a *motion head*, and a *semantic head*.

The Gaussian head regresses the geometric and appearance parameters of 3D Gaussians, specifically the pixel-aligned depth $d \in \mathbb{R}$, rotation represented by a unit quaternion $\mathbf{q} \in \mathbb{R}^4$, scale $\mathbf{s} \in \mathbb{R}^3$, opacity $\alpha \in [0, 1]$, and color $\mathbf{c} \in \mathbb{R}^3$, collectively forming a 12-dimensional parameter vector per Gaussian primitive.

Each Gaussian primitive is parameterized by position, scale, rotation (quaternion), opacity, RGB color, and an auxiliary depth value. We use the following activation functions to map raw network outputs to valid physical ranges:

- **Scale:** $\text{scale} = \min(\exp(x + \text{scale_offset}), 0.5)$, where $\text{scale_offset} = -0.693$ (i.e., $\log(0.5)$). This initialization biases the model to start from relatively large Gaussians and shrink during training, which we empirically find beneficial for stable self-supervised learning of motion.
- **Opacity:** $\sigma = \text{sigmoid}(x - 2.0)$, following GS-LRM [76], which encourages sparse initialization (low opacity) and reduces floaters.
- **RGB:** $\mathbf{c} = \text{sigmoid}(x)$, clamping colors to $[0, 1]$.
- **Depth:** $d = \text{near} + \text{sigmoid}(x) \cdot (\text{far} - \text{near})$, with $\text{near} = 0.2$ and $\text{far} = 400$, ensuring depth values lie within a physically plausible range.
- **Quaternion:** No activation is applied.

The motion head predicts 12-dimensional third-order motion properties. For each order $l \in \{1, 2, 3\}$, it outputs a scalar velocity magnitude and a 3-dimensional directional vector, resulting in $4 \times 3 = 12$ dimensions.

The semantic head produces a 64-dimensional semantic feature map intended for novel-view feature rendering. This feature map is subsequently refined by an auxiliary MLP decoder that expands its dimensionality from 64 to 512, ensuring compatibility with the LSeg feature space.

7. Why We Choose LSeg

Within the framework of feature distillation, the capability of teacher features is crucial for the final semantic reconstruction performance of the model. In order to enable our features to possess language alignment capability, we select three types of CLIP-related features and conduct experimental comparisons.

□ **MaskCLIP** [9]: Standard CLIP [45] computes similarity only between text and global visual feature during contrastive learning, resulting in the local visual features not being strictly aligned with text. MaskCLIP is a CLIP variant that achieves alignment between local features and text. However, its features undergo significant spatial downsampling, yielding semantically condensed but geometrically distorted representations. In SAB3R [5], MaskCLIP features are processed via FeatUp [15], which upsamples the low-resolution features to restore geometric fidelity. As shown in the second row of Figure 7, in our experiments, this upsampling method can accurately restore the edges of some instances. However, it tends to cause feature confusion, which easily interferes with feature learning.

□ **SAM-CLIP:** We use SAM-CLIP to denote instance-level CLIP features obtained by extracting CLIP features from SAM-segmented regions. Similar to PE3R [19], we use SAM to segment images and extract CLIP features from the segmented regions. Meanwhile, we employ SAM2 [46] to perform instance ID alignment across different frames and views, and conduct feature aggregation for identical instances. As shown in the third row of Figure 7, benefiting from the segmentation prior, the instance boundaries in the SAM-CLIP feature map are extremely clear. However, the segmentation prior also introduces several drawbacks, such as the presence of empty feature regions (where no instances are segmented) and potential feature jumps across frames (resulting from jumps in instance segmentation results across frames). These drawbacks make it less suitable for 4D reconstruction that involves a temporal dimension. Additionally, the complex processing procedure leads to very low efficiency in extracting such features.

□ **LSeg-CLIP** [28]: LSeg-CLIP extends CLIP to the semantic segmentation task and enables text query-driven semantic segmentation. Specifically, LSeg-CLIP calculates the similarity between visual features and text features of various categories, which serves as the basis for category classification. Additionally, LSeg-CLIP adopts a visual encoder with low-magnification downsampling, allowing its features to retain a certain degree of geometric structure. As

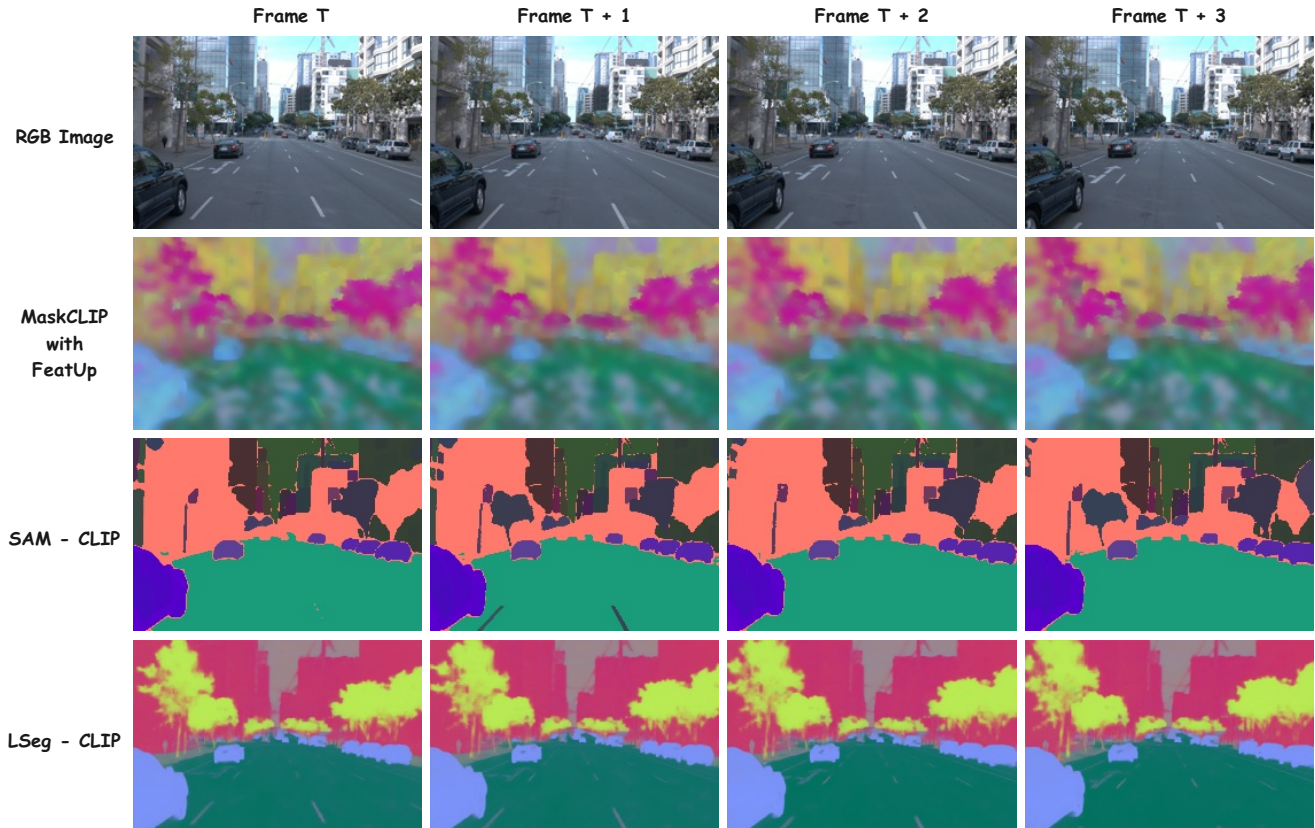


Figure 7. Comparison of different language-aligned features. The first row is the input consists of a set of images from adjacent frames, the next three rows correspond to the three types of features for each frame, respectively.

shown in the last row of Figure 7, in our experiments, LSeg-CLIP features exhibit strong semantic expression capabilities, with sufficiently unified semantics for each category. Although its instance boundaries are less clear than those of SAM-CLIP, it possesses advantages that SAM-CLIP lacks: the absence of feature-less regions, the continuity between inter-frame features, and the efficiency of feature extraction. After comprehensive comparison, we adopt LSeg-CLIP features as our teacher features to endow Gaussian primitives with the capability of semantic reconstruction.

8. Results in more outdoor datasets

We extend SLARM to two more large-scale driving datasets—NuScenes [1] and Argoverse2 [59]. As shown in Table 4, SLARM consistently outperforms STORM in dynamic scene reconstruction.

9. More Experiment Results

We present additional image and video results captured from novel viewpoints across a diverse set of dynamic scenarios. These include relatively simple cases—such as

Table 4. Comparison on NuScenes and Argoverse2 Datasets.

Method	NuScenes		Argoverse2	
	PSNR \uparrow	D-RMSE \downarrow	PSNR \uparrow	D-RMSE \downarrow
STORM	26.25	4.78	26.13	9.04
SLARM-F	26.71	4.24	26.49	8.65
SLARM-W	<u>26.42</u>	<u>4.29</u>	<u>26.26</u>	<u>8.71</u>

scenes with sparse moving objects exhibiting smooth motion (see Figure 8)—as well as highly complex environments characterized by multiple simultaneously moving people and heterogeneous dynamic objects (see Figures 9–11). Further supplementary results, provided in the accompanying folder, corroborate that our method, SLARM, consistently delivers robust and high-fidelity reconstructions across this spectrum of scene complexity. Notably, SLARM preserves strong temporal coherence, accurate geometry, and photorealistic detail under both subtle motions and intricate multi-agent interactions, underscoring its generalizability and practical efficacy in real-world dynamic settings.

Additional videos results are available in our page <https://kevinchiu19.github.io/SLARM/>.

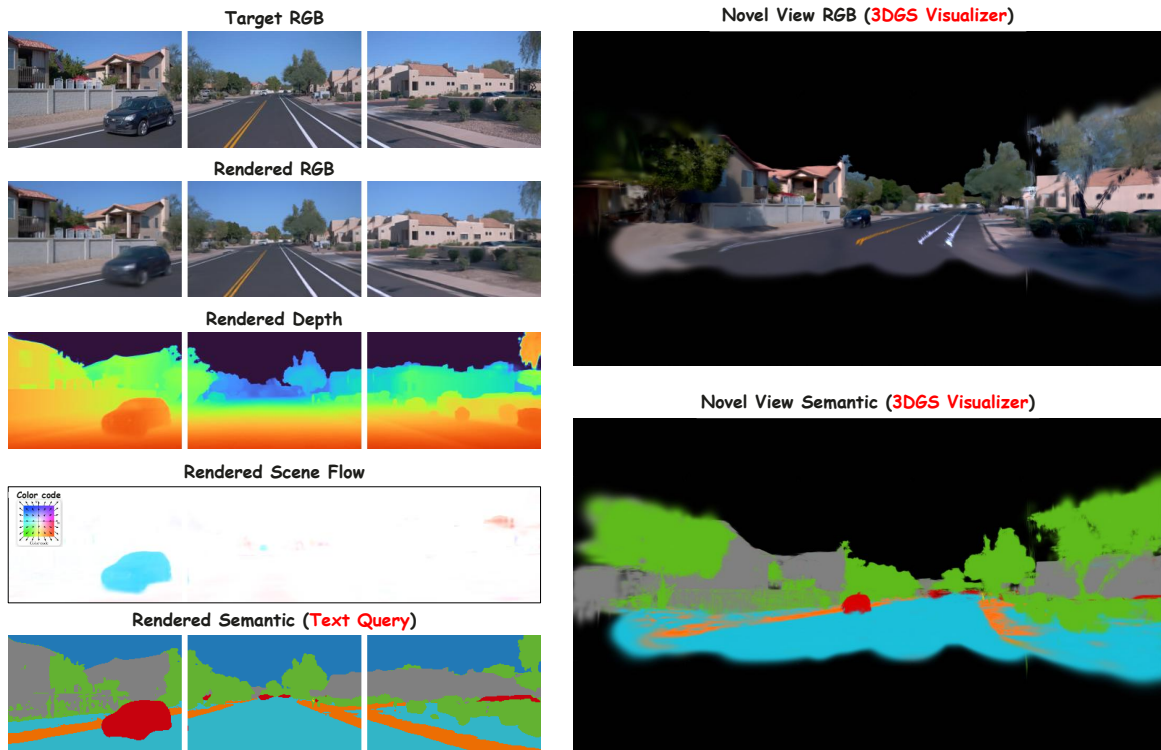


Figure 8. Qualitative results on a simple outdoor scene: left shows rendered RGB, depth, 3D scene flow, and semantic map from predicted 4DGS; right displays a novel view of the 4DGS in a 3DGS visualizer.

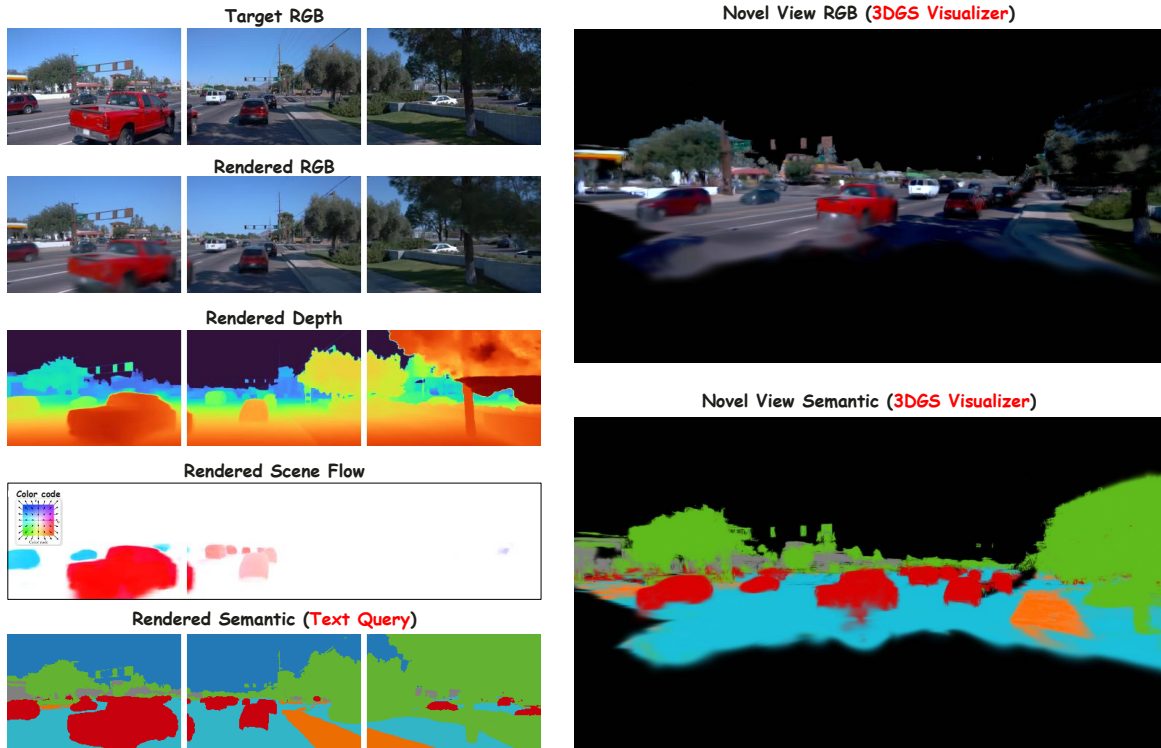


Figure 9. Qualitative results on a complex outdoor scene: left shows rendered RGB, depth, 3D scene flow, and semantic map from predicted 4DGS; right displays a novel view of the 4DGS in a 3DGS visualizer.

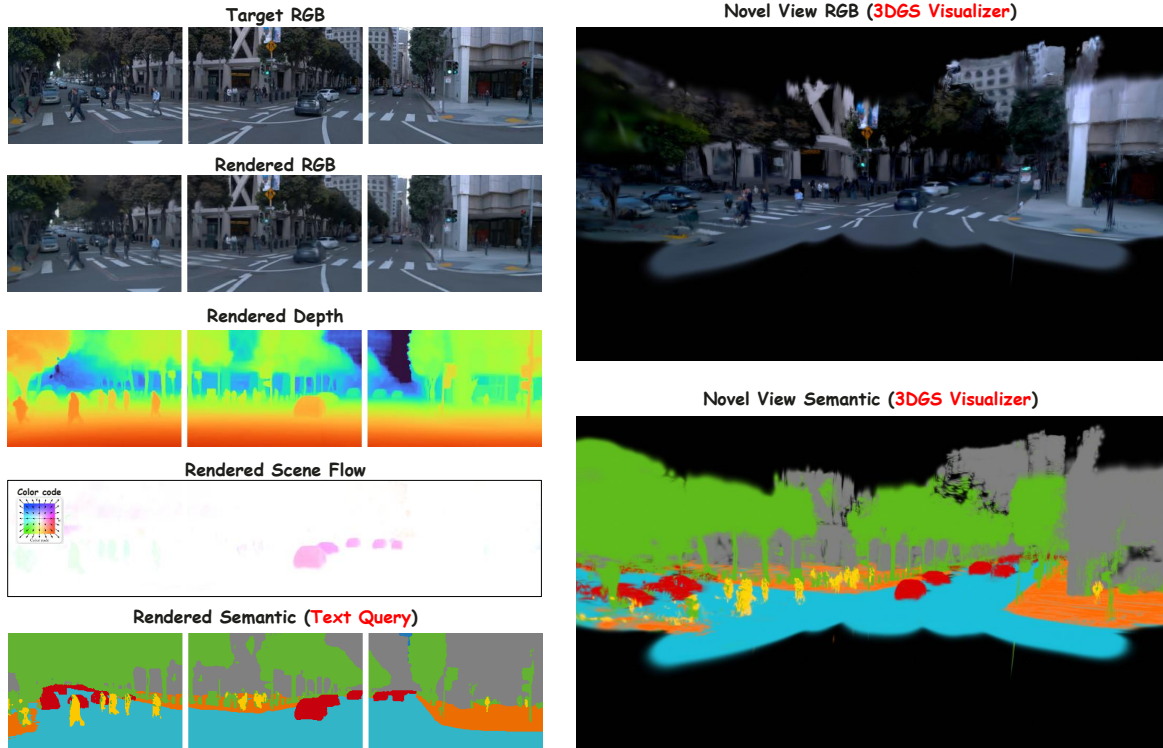


Figure 10. Qualitative results on a complex outdoor scene: left shows rendered RGB, depth, 3D scene flow, and semantic map from predicted 4DGS; right displays a novel view of the 4DGS in a 3DGS visualizer.

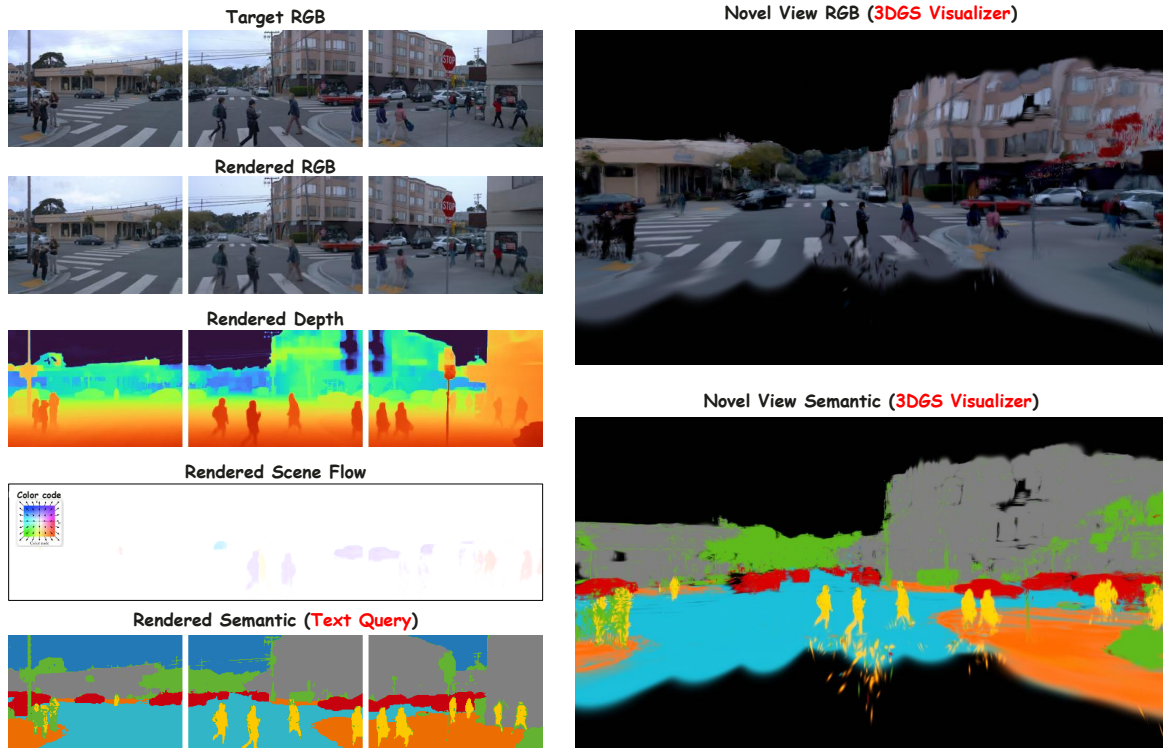


Figure 11. Qualitative results on a complex outdoor scene: left shows rendered RGB, depth, 3D scene flow, and semantic map from predicted 4DGS; right displays a novel view of the 4DGS in a 3DGS visualizer.